Journal of Quality Measurement and Analysis *JQMA* 22(1) 2026, 55-69
e-ISSN: 2600-8602 *http://www.ukm.my/jqma*
https://doi.org/10.17576/jqma.2201.2026.04

STABILITY ANALYSIS OF MHD STAGNATION POINT FLOW TOWARDS A PERMEABLE STRETCHING/SHRINKING SHEET IN A POROUS MEDIUM WITH THE HEAT GENERATION/ABSORPTION

(*Analisis Kestabilan bagi Aliran Titik Genangan MHD Terhadap Permukaan Telap Meregang/Mengecut dalam Bahantara Berliang dengan Penjanaan/Penyerapan Haba*)

KHAIRY ZAIMI*, LIAQUAT ALI LUND, FATINNABILA KAMAL,
UBAIDULLAH YASHKUN, SULIADI FIRDAUS SUFAHANI & MOHAMMAD FERDOWS

ABSTRACT

This research explores the magnetohydrodynamic (MHD) stagnation-point flow (SPF) over a permeable surface that either stretches or shrinks, incorporated into a permeable surface while also accounting for internal heat generation and absorption effects. Through a similarity transformation, the complex nonlinear partial differential equations (PDEs) describing the flow as well as heat transfer are simplified into a system of nonlinear ordinary differential equations (ODEs). Consequently, these equations are numerically solved with MATLAB's boundary value problem solver, *bvp4c*. The obtained outcomes include detailed analyses into velocity as well as temperature profiles, along with evaluations of the skin friction coefficient (SFC), as well as the local dimensionless heat transfer rate, which quantify surface drag and the rate of heat transfer, respectively. Notably, for the shrinking sheet, the model results to dual solutions, whereas for the stretched sheet, only a single solution is obtained.The findings indicate that an improve in the permeability coefficient R leads to enhancements in both SFC and the heat transfer rate at the surface. Conversely, a rise in the heat generation or absorption parameter results in a decline in the surface heat transfer rate. Furthermore, a temporal stability analysis confirms that the primary (first) solution remains stable over time, while the secondary solution is found to be unstable.

Keywords: dual solutions; stability analysis; heat generation/absorption; porous medium

ABSTRAK

Aliran titik genangan magnetohidrodinamik (MHD) terhadap kepingan meregang atau mengecut boleh telap dalam bahantara berliang, dengan mengambil kira kesan penjanaan/penyerapan haba. Persamaan pembezaan separa menakluk tak linear (PPS) dijelmakan kepada satu sistem persamaan pembezaan biasa tak linear (PPB) menggunakan penjelmaan keserupaan. Persamaan yang telah dijelmakan ini kemudian diselesaikan secara berangka mengguna pakai penyelesai masalah nilai sempadan (bvp4c) dalam perisian MATLAB. Keputusan berangka merangkumi profil-profil halaju dan suhu, termasuk pekali geseran kulit serta nombor Nusselt setempat, yang menunjukkan kadar pemindahan haba pada permukaan. Didapati bahawa penyelesaian dual wujud bagi kepingan mengecut, manakala kepingan meregang menghasilkan penyelesaian unik. Hasil kajian menunjukkan bahawa pekali geseran kulit serta kadar pemindahan haba pada permukaan meningkat dengan peningkatan nilai parameter ketelapan R. Sebaliknya, kadar pemindahan haba berkurang apabila parameter penjanaan/penyerapan haba Q meningkat. Analisis kestabilan temporal selanjutnya mendapati bahawa penyelesaian pertama adalah stabil, manakala penyelesaian kedua adalah tidak stabil.

Kata kunci: penyelesaian dual; analisis kestabilan; penjanaan/penyerapan haba; bahantara berliang

1. Introduction

The research concerning fluid flow as well as heat transfer in a permeable domain adjacent to a stretching/shrinking surface (SSS), particularly when internal heat generation or absorption is involved, is significantly importance because of its broad engineering and industrial applications. This research aids in optimizing essential heat transfer processes, which includes boundary layer (BL) behavior during liquid film condensation, aerodynamic extrusion of plastic sheets, extrusion of metals and polymers, thermal insulation, metal spinning, and geophysical flow. The interaction between fluid dynamics and heat transfer with regard to a permeable domain, accounting for heat generation or absorption, significantly influences efficiency and stability in various engineering systems. For example, in industries such as metallurgy and chemical processing, the accuracy of heat control during the stretching process is important for material quality and energy savings. Furthermore, heat generation also crucial for cooling electronic devices (Merkin *et al.* 2017).

Among the recent studies conducted over heat transfer and flow problem towards SSS in a permeable domain include a study by Khan *et al.*(2020), Hakim *et al.* (2023), Nagaraju *et al.* (2024), Khalil *et al.* (2024) as well as Shahzad *et al.* (2024). For example, Hakim *et al.* (2023) examined SPF as well as heat transfer in a permeable domain, given the heat generation over an exponentially SSS, finding that the local dimensionless heat transfer rate, resembling the surface heat transfer rate, reduces with an increase in the heat generation parameter but enhances with a greater permeability coefficient. Nagaraju *et al.* (2024) analyzed the Jeffrey fluid BL flow over a SSS in a permeable domain, concluding that for both cases, a rise in the permeability coefficient decreases velocity. Meanwhile, Khalil *et al.* (2024) assessed the behavior of nanofluids in MHD, mass transfer, and Joule heating over an exponentially stretched sheet within a permeable domain under thermal radiation effects, observing that higher permeability decreases velocity but raises fluid temperature due to the permeable domain's rsistance on fluid flow and thickening of the thermal BL. Shahzad *et al.* (2024) explored how melting influences heat as well as mass transfer in a Darcy-Forchheimer permeable domain with nanofluids at the stagnation point of a horizontal cylindrical surface under the effect of MHD, reporting that the surface drag (SFC) lowers as the permeability coefficient rises. Recently, many researchers have carried out stability analysis for a variety of types of flow as well as heat transfer problems across different types of surfaces and fluids as well as boundary conditions (BC). The primary objective of this analysis is to assess the stable and reliable solution among the dual solutions obtained. Among the studies involved for example by Jamrus *et al.* (2024) and Puspanathan *et al.* (2024). The combination of these effects SSS, heat generation/absorption, and flow via a permeable domain creates a more realistic model that reflects conditions found in various engineering and industrial systems. Analyzing their combined influence is important because it helps to improve thermal management in energy systems and electronics. The impacts of heat generation/absorption as well as porous media are crucial in managing excess heat in electronic cooling systems, solar collectors, and nuclear reactors. SSS is also encountered in thin film technology and extrusion processes (Bejan 2013; Nield & Bejan 2017). Flows through porous media with heat generation/absorption are important in biological flows (e.g., tissue perfusion), chemical reactors, and filtration units (Pop & Ingham 2001; Vafai 2015).

In this study, the numerical analysis of MHD SPF as well as heat transfer toward a SSS permeable in a permeable domain, accounting for heat generation or absorption, is conducted. Heat generation or absorption within a permeable domain is commonly encountered in various industrial and technological processes, including processes involving chemical reactions, and problems associated with dissociating fluids (Vajravelu & Nayfeh 1992). The present research extends the earlier investigation conducted by Aman *et al.* (2013), who explored the two-dimensional SPF over a SSS in a viscous, incompressible fluid, incorporating the influences of magnetohydrodynamic (MHD) effects along with velocity as well as thermal slip conditions. They reported that the SFC lowers, while the surface heat transfer rate rises when velocity and thermal slip effects are included. Dual solutions were identified for the shrinking sheet, while only a single solution existed for the stretched sheet. Furthermore, Aman *et al.* (2013) did not account for the impacts of heat absorption/generation and did not conduct a stability analysis in identifying the stable and physically meaningful solution. This study differs from Aman *et al.* (2013) by considering the flow on a SSS permeable at the boundary with heat generation/absorption effects in a permeable domain, and reporting the presence of dual solution. Other than that, a stability analysis is conducted to evaluate which solutions are stable as well as physically significant. The impact of the the permeability coefficient and heat absorption/generation parameters on SFC, including velocity and temperature profiles, is examined and discussed.

2. Mathematical Formulation

The 2D SPF and heat transfer towards a linearly SSS in an incompressible viscous fluid is examined, as depicted in Figure 1. Note that the Cartesian coordinates with respect to x and y are considered with the origin origin O located at the stagnation point. It is expressed so that the $x-$axis runs along the sheet. Meanwhile, the $y-$axis is oriented perpendicular to it. Here, we assume that the free stream velocity is given by $U(x) = ax$, in which a refers to positive constant. Moreover, the velocity with respect to the SSS is given by $U_w(x) = cx$ in which $c > 0$ matches to the stretched sheet whereas $c < 0$ expresses the shrinking sheet together with the slip velocity at the boundary. A constant magnetic flux density B_0 is applied from outside in the positive direction along $y-$ axis. Since the magnetic dimensionless inertial–viscous ratio is small, the induced magnetic flux density is very weak and can be neglected.

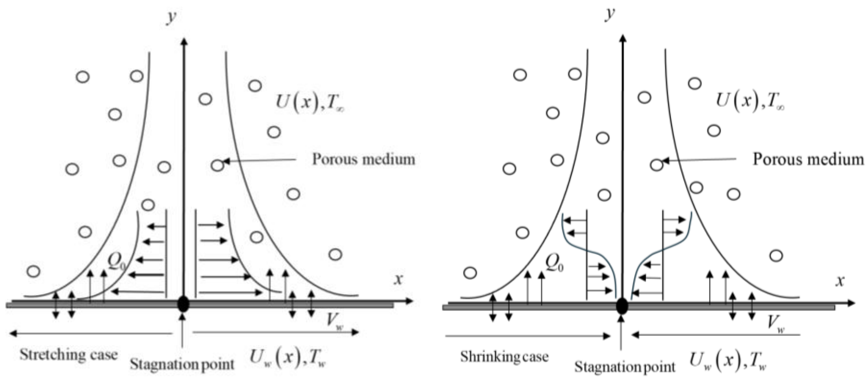

Figure 1: Physical model as well as coordinate system for the suggested problem.

Based on the assumptions stated while employing the BL approximation, the governing equations for continuity, momentum, as well as energy are given as (Aman *et al.* 2013; Ishak *et al.* 2009; Bhattacharyya *et al.* 2011)

$$\frac{\partial u}{\partial x}+\frac{\partial v}{\partial y}=0, \tag{1}$$

$$u\frac{\partial u}{\partial x}+v\frac{\partial u}{\partial y}=U\frac{dU}{dx}+\nu\frac{\partial^2 u}{\partial y^2}+\frac{\sigma B_0^2}{\rho}\left(U-u\right)+\frac{\nu}{K}\left(U-u\right), \tag{2}$$

$$u\frac{\partial T}{\partial x}+v\frac{\partial T}{\partial y}=\alpha\frac{\partial^2 T}{\partial y^2}+\frac{Q_0}{\rho c_p}\left(T-T_\infty\right), \tag{3}$$

subject to the BC:

$$u=U_w\left(x\right)+L\left(\partial u/\partial y\right),\quad v=V_w,\quad T=T_w+S\left(\partial T/\partial y\right)\ \text{at}\ y=0, \tag{4}$$
$$u\to U\left(x\right),\quad T\to T_\infty\quad \text{as}\ y\to\infty.$$

Given the equations above, $\left(u,v\right)$ denotes the fluid velocity components along $\left(x,y\right)$ directions, T denotes the fluid temperature, T_w and T_∞ denote the temperature at the surface as well as the ambient temperature, accordingly, ν refers to the kinematic viscosity, α refers to the thermal diffusion coefficient, ρ resembles the fluid density, σ refers to the electrical conductivity, Q_0 resembles the temperature-dependent heat generation/absorption coefficient, K refers to the coefficient of permeability of the permeable domain, L denotes the proportional coefficient of velocity slip, S refers to the proportional coefficient of thermal slip while V_w denotes the uniform surface mass flux where $V_w>0$ resembles the suction, while $V_w<0$ resembles the injection at the boundary.

To derive a similarity solution for the governing Eqs. (1)–(3) under the BC (4), the similarity transformation given below is introduced (Aman *et al.* 2013)

$$\eta=\left(\frac{U}{\nu x}\right)^{1/2}y,\ \psi=\left(\nu xU\right)^{1/2}f\left(\eta\right),\ \theta\left(\eta\right)=\frac{T-T_\infty}{T_w-T_\infty}, \tag{5}$$

in which η resembles the independent similarity variable, $f\left(\eta\right)$ as well as $\theta\left(\eta\right)$ denote the dimensionless stream function as well as dimensionless temperature, accordingly. Meanwhile, ψ refers to the stream function referred to as $u=\partial\psi/\partial y$ as well as $v=-\partial\psi/\partial x$, which holds the continuity Eq. (1). Utilizing Eq. (5), the velocity can be written as

$$u=axf'\left(\eta\right)\ \text{as well as}\ v=-\left(\nu a\right)^{1/2}f\left(\eta\right), \tag{6}$$

in which primes sign (') represents differentiation with regards to η. Hence, substituting Eqs. (5) and (6) into Eqs. (2) and (3) results in the non-linear ODEs given below:

$$f'''+ff''+1-f'^2+\left(M+\mathrm{R}\right)\left(1-f'\right)=0, \tag{7}$$

$$\frac{1}{\mathrm{Pr}}\theta''+f\theta'+\mathrm{Q}\theta=0, \tag{8}$$

in which $M=\sigma B_0^2/\rho a$ refers to the magnetic flux density parameter, $\mathrm{Pr}=\nu/\alpha$ refers to the Prandtl number, R expresses the permeability coefficient while Q refers to the dimensionless heat generation/absorption coefficient parameter with $(\mathrm{Q}>0)$ correlates to heat generation, while $(\mathrm{Q}<0)$ correlates to absorption case.

The BC (4) reduce to:

$$\begin{aligned} &f(0)=\gamma, \quad f'(0)=\varepsilon+\delta f''(0), \quad \theta(0)=1+\beta\theta'(0), \\ &f'(\infty)\to 1, \ \ \theta(\infty)\to 0, \end{aligned} \tag{9}$$

in which $\gamma=-V_w/(a\nu)^{1/2}$ refers to the suction/injection parameter with $\gamma>0$ resembles suction, $\gamma<0$ represents injection and $\gamma=0$ is for the case of impermeable surface. Meanwhile, $\varepsilon=c/a$ denotes the stretching/shrinking parameter (SSP) with $\varepsilon>0$ represents the stretched sheet while $\varepsilon<0$ resembles the shrinking sheet, $\delta=L(a/\nu)^{1/2}$ refers to the velocity slip parameter and $\beta=S(a/\nu)^{1/2}$ denote the thermal slip parameter.

The physical quantities considered in this paper are SFC C_f as well as Nu_x, that are expressed as (Aman *et al.* 2013)

$$C_f=\frac{\tau_w}{\rho U^2/2}, \quad Nu_x=\frac{xq_w}{k\left(T_w-T_\infty\right)}, \tag{10}$$

in which τ_w refers to the surface shear stress, while q_w refers to the surface heat flux expressed as

$$\tau_w=\mu\left(\frac{\partial u}{\partial y}\right)_{y=0}, \quad q_w=-k\left(\frac{\partial T}{\partial y}\right)_{y=0}. \tag{11}$$

Note that μ as well as k denote the fluid's dynamic viscosity as well as thermal conductivity, accordingly. By utilizing Eqs. (5), (10) and (11), we gained

$$1/2\, C_f \,\mathrm{Re}_x^{1/2}=f''(0), \quad Nu_x/\mathrm{Re}_x^{1/2}=-\theta'(0), \tag{12}$$

in which $\mathrm{Re}_x=Ux/\nu$ denotes the local dimensionless inertial–viscous ratio.

3. Stability Analysis

To assess the stability regarding the various solutions associated with the boundary value problem described in Eqs. (7)–(9), a detailed stability analysis is carried out. The methodology follows the approaches outlined by Roşca and Pop (2013), Weidman *et al.* (2006), and Merkin (1986). In particular, the introduction of a non-dimensional time parameter, as proposed by Weidman *et al.* (2006), transforms the flow into an unsteady and potentially unstable regime. While Eq. (1) remains unchanged, the unsteady counterparts of Eqs. (2) and (3) are adopted for the current investigation. The modified governing equations used in the unsteady analysis are presented below.

$$\frac{\partial u}{\partial t}+u\frac{\partial u}{\partial x}+v\frac{\partial u}{\partial y}=U\frac{dU}{dx}+\nu\frac{\partial^2 u}{\partial y^2}+\frac{\sigma B_0^2}{\rho}\left(U-u\right)+\frac{\nu}{K}\left(U-u\right), \tag{13}$$

$$\frac{\partial T}{\partial t}+u\frac{\partial T}{\partial x}+v\frac{\partial T}{\partial y}=\alpha\frac{\partial^2 T}{\partial y^2}+\frac{Q_0}{\rho c_p}\left(T-T_\infty\right), \tag{14}$$

in which t refers to time. A new similarity transformation for unsteady flow is introduced as follows:

$$\eta=\left(\frac{U}{\nu x}\right)^{\frac{1}{2}}y,\ u=axf'\left(\eta,\tau\right),\ v=-\left(\nu a\right)^{\frac{1}{2}}f\left(\eta,\tau\right),\ \theta\left(\eta,\tau\right)=\frac{T-T_\infty}{T_w-T_\infty},\ \tau=at. \tag{15}$$

By rewriting Eq. (15) into Eqs. (13) and (14), we obtain

$$\frac{\partial^3 f}{\partial\eta^3}+f\frac{\partial^2 f}{\partial\eta^2}-\left(\frac{\partial f}{\partial\eta}\right)^2+\left(M+\mathrm{R}\right)\left(1-\frac{\partial f}{\partial\eta}\right)+1-\frac{\partial^2 f}{\partial\eta\partial\tau}=0, \tag{16}$$

$$\frac{1}{\mathrm{Pr}}\frac{\partial^2\theta}{\partial\eta^2}+f\frac{\partial\theta}{\partial\eta}+\mathrm{Q}\theta-\frac{\partial\theta}{\partial\tau}=0, \tag{17}$$

subject to the BC:

$$f\left(0,\tau\right)=\gamma,\ \frac{\partial f}{\partial\eta}\left(0,\tau\right)=\varepsilon+\delta\frac{\partial^2 f}{\partial\eta^2}\left(0,\tau\right),\ \theta\left(0,\tau\right)=1+\beta\frac{\partial^2\theta}{\partial\eta^2}\left(0,\tau\right), \tag{18}$$

$$\frac{\partial f}{\partial\eta}\left(\eta,\tau\right)=1,\ \theta\left(\eta,\tau\right)=0,\ \text{as }\eta\to\infty.$$

As per Weidman *et al.* (2006), to test stability behavior, the basic flow $f\left(\eta\right)=f_0\left(\eta\right)$ and $\theta\left(\eta\right)=\theta_0\left(\eta\right)$ that is gained from Eqs. (16) and (17) will be perturbed with exponential form

$$\begin{aligned} f\left(\eta,\tau\right)&=f_0\left(\eta\right)+e^{-\lambda\tau}F\left(\eta,\tau\right),\\ \theta\left(\eta,\tau\right)&=\theta_0\left(\eta\right)+e^{-\lambda\tau}G\left(\eta,\tau\right). \end{aligned} \tag{19}$$

Note that, λ refers to the unknown eigenvalue, $F\left(\eta,\tau\right)$ as well as $G\left(\eta,\tau\right)$ denote small relative to $f_0\left(\eta\right)$ and $\theta_0\left(\eta\right)$. Thus, the eigenvalue problem (16)-(18) solutions yield an infinite series of eigenvalues. Provided that λ is negative, disturbances initially grow, indicating that the flow is unstable over time. However, if λ is positive, disturbances initially decay, making the flow stable. Here, by rewriting Eq. (19) into Eqs. (16) and (17), the linearized equations are acquired.

$$F'''+f_0F''+f_0''F-\left(2f_0'-\lambda+M+\mathrm{R}\right)F'=0, \tag{20}$$

$$\frac{1}{\mathrm{Pr}}G''+f_0G'+\theta_0'F+\left(\mathrm{Q}+\lambda\right)G=0, \tag{21}$$

subject to the BC

$$F\left(0,\tau\right)=0,\ \frac{\partial F}{\partial \eta}\left(0,\tau\right)=\delta\frac{\partial^{2} F}{\partial \eta^{2}}\left(0,\tau\right),\ G\left(0,\tau\right)=\beta\frac{\partial G}{\partial \eta}\left(0,\tau\right). \tag{22}$$

We obtained new BC (22) by substituting Eq. (19) into the BC (18) and applying the BC (9) for the steady-state solutions.

4. Result Interpretation

The nonlinear ODEs (7) and (8), coupled with the BC specified in equation (9), were addressed numerically employing MATLAB's boundary value problem solver, *bvp4c*. Through this numerical approach, comprehensive results were obtained to evaluate the influence with regard to various dimensionless parameters on key flow and thermal characteristics, including SFC, the local dimensionless heat transfer rate (which measures the heat transfer rate at the surface), alongside the velocity $f'\left(\eta\right)$ and temperature $\theta\left(\eta\right)$ distributions within the BL. Particular attention was given to analyzing how changes in the permeability coefficient R as well as the heat generation or absorption parameter Q influence the fluid dynamics and heat transfer behavior in the system.

To ensure the validity and reliability of the present numerical solutions, a systematic comparison was conducted against previously published results for the shrinking sheet scenario. Specifically, values of SSC ($f''\left(0\right)$) for selected SSP ε values were compared with those revealed by Aman *et al.* (2013), Bhattacharyya *et al.* (2011), and Wang (2008). These comparative results are compiled in Table 1, which demonstrates strong consensus between the current and prior studies. This strong correlation not only validates the computational methodology employed but also instills confidence in the accuracy of other numerical data presented throughout this work.

Furthermore, the analysis highlights the sensitivity of flow and thermal profiles to variations in permeability and internal heat effects, providing deeper insight into the underlying physical processes. The comprehensive parametric study thus offers valuable guidance regarding the design as well as optimization of engineering systems incorporating porous media with MHD and thermal generation or absorption phenomena.

Table 2 displays the values of SFC as well as Nu_x for several the permeability coefficient R and the SSP ε values when $\gamma, \mathrm{Pr}, \delta, \beta, \mathrm{Q}$ and M are fixed. It can be observed that SFC $1/2\,C_f\,\mathrm{Re}_x^{1/2}$ alongside the local dimensionless heat transfer rate $Nu_x/\mathrm{Re}_x^{1/2}$ values increase with increasing of R. Table 3 displays the value with regard to the local dimensionless heat transfer rate for several values of the heat generation/absorption parameter Q and SSP ε when $\gamma, \mathrm{Pr}, \delta, \beta$, R and M are fixed. It is considered that the local dimensionless heat transfer rate values decrease when the heat generation/absorption parameter Q increases. As indicated in Table 3, SFC values remain unaffected by the heat generation/absorption parameter Q. Additionally, Tables 2 and 3 confirm that dual solutions exist in the shrinking scenario, with the second solutions shown in brackets ( ).

Table 1: Comparison concerning the values of $f''(0)$ when $M = \mathrm{R} = \delta = \beta = \mathrm{Q} = 0$ and $\Pr = 1$ for shrinking region $(\varepsilon < 0)$.

ε	Aman *et al.* (2013)	Wang (2008)	Bhattacharyya *et al.* (2011)	Present results
-0.25	1.4022	1.40224	1.402241	1.402240
-0.35				1.449751
-0.4	1.4686			1.468613
-0.615	1.5072		1.507241	1.507240
-0.75	1.4893	1.4893	1.489298	1.489298
-0.9				1.418077
-1	1.3288(0)	1.32882(0)	1.328817(0)	1.328816(0)
-1.11				1.168153(0.059972)
-1.12				1.148567(0.071979)
-1.14				1.105755(0.100205)
-1.15	1.0822(0.1167)	1.08223(0.116702)	1.082232(0.116673)	1.082231(0.116702)
-1.16				1.057031(0.135039)
-1.18	1.0004(0.1784)			1.000449(0.178453)
-1.19				0.968216(0.204181)
-1.21				0.892092(0.267886)
-1.22				0.845110(0.308849)
-1.23				0.787437(0.360623)
-1.2465	0.5543(0.5543)	0.55430	0.554286(0.554286)	0.554296(0.554296)

( ) second solution

Table 2: Values of $1/2\,C_f\,\mathrm{Re}_x^{1/2}$ and $Nu_x/\mathrm{Re}_x^{1/2}$ for distinct values with regard to the permeability coefficient R when $\gamma = 0.5,\ M = \mathrm{Q} = 0.1$ and $\Pr = \delta = \beta = 1$.

ε	R	$1/2\,C_f\,\mathrm{Re}_x^{1/2}$	$Nu_x/\mathrm{Re}_x^{1/2}$
1	0	0	0.521733194
	0.1	0	0.521733194
	0.2	0	0.521733
2	0	-0.668212	0.535987
	0.1	-0.671120	0.535783
	0.2	-0.673942	0.535586
3	0	-1.355080	0.547947
	0.1	-1.360203	0.547620
	0.2	-1.365193	0.547301
-2	0	1.799996 (0.462496)	0.447261 (-0.184220)
	0.1	1.822207 (0.403434)	0.450139 (-0.207766)
	0.2	1.842589 (0.347013)	0.452712 (-0.208246)
-3	0	2.201553 (1.422758)	0.380478 (0.091316)
	0.1	2.264048 (1.313771)	0.392260 (0.016784)
	0.2	2.314359 (1.217065)	0.401099 (-0.052790)

( ) second solution

Table 3: Values of $1/2\, C_f \, \mathrm{Re}_x^{1/2}$ and $Nu_x / \mathrm{Re}_x^{1/2}$ for different values concerning the heat generation/absorption parameter Q when $\gamma = 0.5,\ M = \mathrm{R} = 0.1$ and $\Pr = \delta = \beta = 1$.

ε	Q	$1/2\, C_f \, \mathrm{Re}_x^{1/2}$	$Nu_x / \mathrm{Re}_x^{1/2}$
1	-0.5	0	0.577395
	0	0	0.532945
	0.1	0	0.521733
2	-0.5	-0.671120	0.586484
	0	-0.671120	0.545870
	0.1	-0.671120	0.535783
3	-0.5	-1.360203	0.594359
	0	-1.360203	0.556824
	0.1	-1.360203	0.547620
-2	-0.5	1.822207 (0.403434)	0.535453 (0.370682)
	0	1.822207 (0.403434)	0.468535 (0.013566)
	0.1	1.822207 (0.403434)	0.450139 (-0.207766)
-3	-0.5	2.264048 (1.313771)	0.506720 (0.401013)
	0	2.264048 (1.313771)	0.418449 (0.144116)
	0.1	2.264048 (1.313771)	0.392260 (0.016784)

( ) second solution

Figures 2-4 portray the variation with regards to SFC alongside local dimensionless heat transfer rate with SSP ε for multiple values of the permeability coefficient R and the heat generation/absorption parameter Q. Figures 2-4 reveal the dual solutions existence for the similarity Eqs. (7)-(8) under the BC (9). Numerical solutions exist in three ranges of SSP ε as illustrated in Figures 2, 3 and 4. Based on Figures 2 and 3, there is a critical value of SSP ε expressed by ε_c in the shrinking region, in which dual solutions exist when $\varepsilon > \varepsilon_c$, a unique solution is acquired when $\varepsilon = \varepsilon_c$ while zero solution is gained when $\varepsilon < \varepsilon_c$. Relying on numerical calculations, the critical values gained are $\varepsilon_c = -3.370, -3.543$ and -3.732 for the permeability coefficient $\mathrm{R}{=}0, 0.1$ and 0.2, respectively as illustrated in Figures 2 and 3. Note that the same critical value obtained $\varepsilon_c = -3.543$ for the heat generation/absorption parameter $\mathrm{Q} = \text{-}0.5, 0$ and 0.1 as shown in Figure 4. In the discussion stated below, the first and second solutions are categorized relying on their appearance in Figure 2. This implies that the first solution possess a greater value of $1/2\, C_f \, \mathrm{Re}_x^{1/2}$ in comparison to the second solution for a given value SSP ε_c. Based on Figures 2 and 3, and Table 2, it can be seen that the values of SFC as well as the local dimensionless heat transfer rate increase due to the permeability coefficient R for the first solution in the shrinking region. This is due to the permeability effect that reduces the flow resistance, increases the fluid flow, and therefore increases the velocity gradients at the surface that is inline with the graph given in Figure 5. Another physical explanation is that increasing the permeability coefficient R causes the decrease of momentum BL thickness, which then rises the flow near the surface. Consequently, SFC rises.

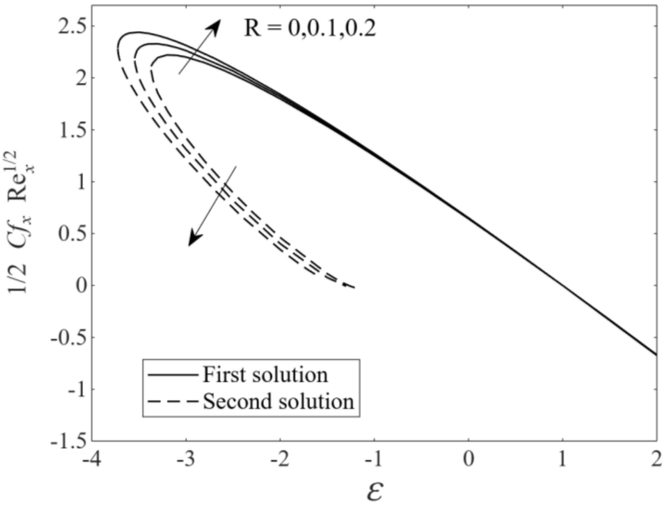

Figure 2: Variation of SFC $1/2\, C_f\, \mathrm{Re}_x^{1/2}$ with ε for distinct values regarding the permeability coefficient R when $\gamma = 0.5$, $M = \mathrm{Q} = 0.1$ and $\mathrm{Pr} = \delta = \beta = 1$.

In Figure 3, it is discovered that the heat transfer rate at the surface rises when the permeability coefficient R rises for the first solution. This is because rising the permeability coefficient R lowers the thermal BL thickness for the first solutions. This in turn rises the temperature gradient at the surface as illustrated in Figure 6. Hence, the heat transfer rate at the surface increases as the permeability coefficient R increases as indicated in Figure 3 and Table 2. Figures 2 as well as 3 also display that the magnitude of critical values of the SSP ε_c for which a solution exists increases with the permeability coefficient R, indicating that this expands the range concerning dual solutions for the similarity Eqs. (7)-(9).

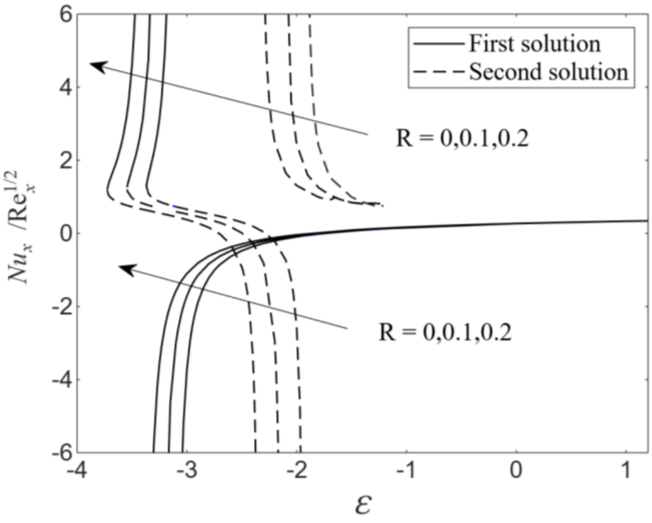

Figure 3: Variation of the local dimensionless heat transfer rate $Nu_x / \mathrm{Re}_x^{1/2}$ with ε for different values of the permeability coefficient R when $\gamma = 0.5$, $M = \mathrm{Q} = 0.1$ and $\mathrm{Pr} = \delta = \beta = 1$.

Figure 4 illustrates how the local dimensionless heat transfer rate varies with SSP ε for several values of the heat generation/absorption parameter Q. As illustrated in Figure 4, the heat transfer rate at the surface decreases as the heat generation/absorption parameter Q rises. This is because a higher heat generation/absorption parameter Q increases the thermal BL thickness for the first solutions and decreases the surface's temperature gradient as illustrated in Figure 7. These findings are consistent with Elbashbeshy *et al.* (2022) who reported that heat generation decreases the local dimensionless heat transfer rate.

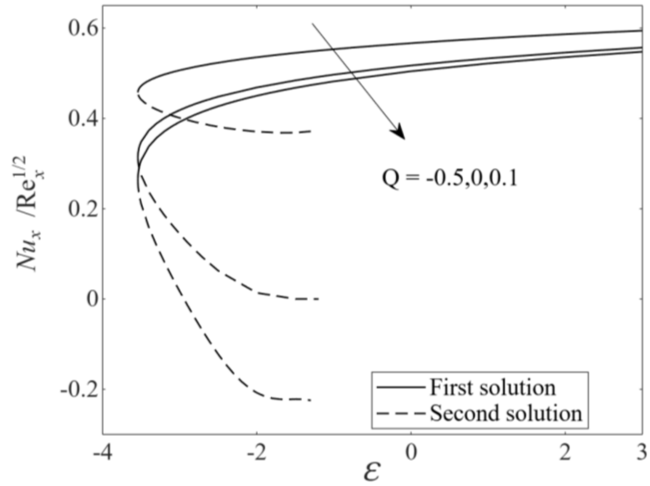

Figure 4: Distinction of the local dimensionless heat transfer rate $Nu_x / \mathrm{Re}_x^{1/2}$ with ε for distinct values with regard to the heat generation/absorption parameter Q when $\gamma = 0.5, M = \mathrm{R} = 0.1$, and $\mathrm{Pr} = \delta = \beta = 1$.

Figures 5 and 6 demonstrate the impact of the the permeability coefficient R on $f'(\eta)$ as well as $\theta(\eta)$ which represent the velocity as well as temperature profiles, respectively. Figure 5 indicates that the velocity rises with the permeability coefficient R for the first solution in the shrinking region. As shown in Figure 5, the first solution depicts the stable as well as physically realizable flow pattern. When the permeability coefficient R increases, it implies that the permeable domain offers less resistance to the flow. This allows fluid to move more freely, increasing the velocity near the surface, which thins the momentum BL and leads to a higher SFC. This behavior is consistent with earlier studies, such as Al Zubi (2018), which reported similar effects in porous BL flows. In contrast, the second solution is typically unstable and represents an alternate, non-physical flow pattern that often exhibits reverse flow characteristics or recirculation zones. When the permeability coefficient R increases, the reduced resistance with regard to the permeable domain may actually destabilize this reverse-type flow, resulting in a reduction in velocity magnitude. In simple terms, while the increased permeability enhances forward flow (as in the first solution), it disrupts the structure of the second solution, making it weaker and less pronounced.

Figure 6 depicts that the temperature lowers with rising of the permeability coefficient R in the shrinking region. This phenomenon occurs due to higher permeability allows more fluid to pass through, assisting faster heat transfer and reducing fluid temperature. Subsequently, the temperature gradient at the surface rises, leading the surface to experience a greater rate of heat transfer, as illustrated in Figure 3 and Table 2.

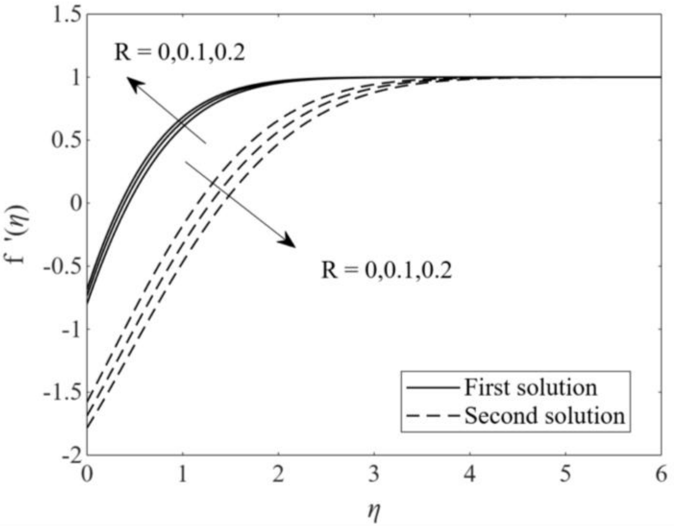

Figure 5: Velocity profiles $f'(\eta)$ for different values of the permeability coefficient R when $\gamma = 0.5, M = \mathrm{Q} = 0.1$, $\mathrm{Pr} = \delta = \beta = 1$ and $\varepsilon = -3$.

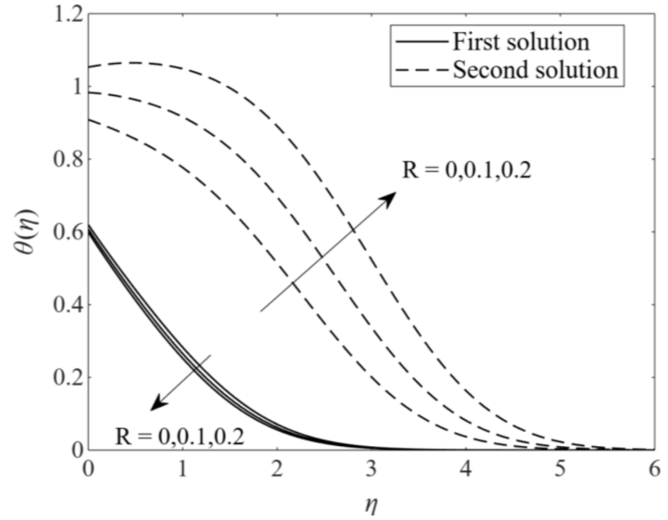

Figure 6: Temperature profles $\theta(\eta)$ for distinct values regarding the permeability coefficient R when $\gamma = 0.5$, $M = \mathrm{Q} = 0.1$ $\mathrm{Pr} = \delta = \beta = 1$ and $\varepsilon = -3$.

Figure 7 illustrates the impact of the heat generation/absorption parameter Q on fluid temperature $\theta(\eta)$. When the heat generation/absorption parameter Q rises, the temperature also rises for the first solution. Physically, rising the value of the heat generation/absorption parameter Q, that is from heat absorption to heat generation, introduces more energy into the system, raising the fluid temperature in BL. As a result, the thermal BL to thicken, reducing the temperature gradient and, consequently, lowering the local dimensionless heat transfer rate, as shown in Figure 4 and Table 3. The velocity as well as temperature profiles presented in Figures 5-7 asymptotically meet the far-field BC (9), confirming the accuracy of the numerical findings. Figures 2-7 and Tables 2-3 demonstrate the occurrence of dual solutions in the shrinking region. Additionally, it is established from Table 3 that the heat generation/absorption parameter Q does not influence the flow field.

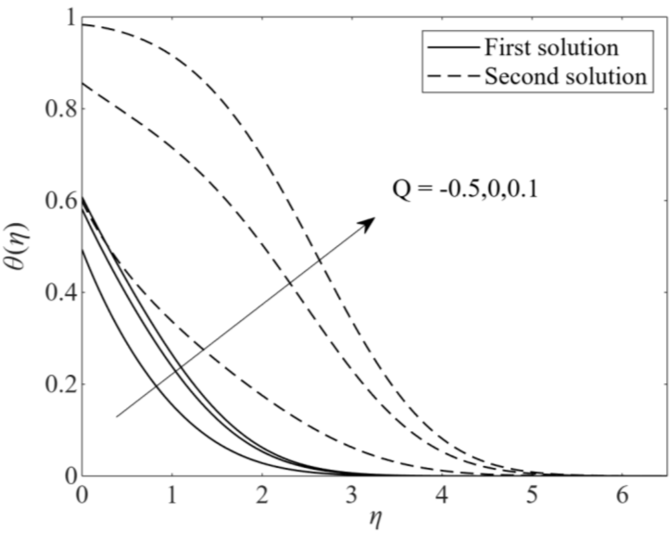

Figure 7: Temperature profiles $\theta(\eta)$ for distinct values of Q when $\gamma = 0.5, M = \mathrm{R} = 0.1$, $\Pr = \delta = \beta = 1$ and $\varepsilon = -3$.

As indicated earlier, the occurrence concerning dual solutions arises within a limited interval corresponding to the shrinking surface regime. A stability analysis is conducted to identify which of these solutions can be physically realized. This procedure entails solving the eigenvalue problem formulated by Eqs. (20) and (21), account to the BC outlined in Eq. (22). Stability is assessed based on the sign of the smallest eigenvalue λ derived from Eq. (19). Specifically, a positive smallest eigenvalue signifies a stable flow configuration, while a negative smallest eigenvalue indicates instability. Over time, positive eigenvalues correspond to the attenuation of perturbations, implying that disturbances diminish and the flow remains steady. Conversely, negative eigenvalues lead to the amplification of disturbances, rendering the flow unstable. Table 4 presents computed smallest eigenvalues for multiple values of SSP ε . It is evident that these eigenvalues are positive for the primary solution, whereas negative for the secondary solution. Therefore, it can be concluded that the first solution maintains stability under temporal evolution, while the second solution is fundamentally unstable.

Table 4: Smallest eigenvalue, λ regarding some values of ε when $\gamma = 0.5, M = 0.1, \mathrm{R} = 0.2$ and $\Pr = \mathrm{Q} = \delta = \beta = 1$.

ε	First solution (Upper branch)	Second solution (Lower branch)
-3	4.6154	0
-3.7	3.7823	-1.0394
-3.71	3.7358	-0.9697
-3.72	3.6620	-0.8576
-3.721	3.6494	-0.8383
-3.722	3.6331	-0.3131
-3.723	3.5977	-0.7584

5. Conclusion

This study has undertaken a comprehensive examination of MHD SPF as well as heat transfer phenomena over a permeable SSS embedded in a permeable domain. Here, the impacts of internal heat generation or absorption were incorporated into the model formulation.

Validation of the numerical results via comparison with current literature under specific limiting conditions demonstrated excellent agreement, thereby establishing the credibility of the present methodology. For a shrinking sheet, the analysis identified dual solutions up to a critical value of the stagnation-point parameter. To assess the physical relevance of these solutions, a temporal stability analysis was performed, which confirmed that the first solution is stable, while the second is unstable. Furthermore, it was discovered that rising the permeability coefficient R results to an expansion in the dual-solution domain. Both SFC as well as the surface heat transfer rate elevate with larger values of R. However, a rose in the absorption parameter or heat generation resulted in a decline in the heat transfer rate at the surface, whereas SFC remained largely unaffected by this thermal parameter.

Acknowledgments

The author extends sincere acknowledgment to the Ministry of Higher Education (MoHE), Malaysia, for the financial assistance provided through the Fundamental Research Grant Scheme (FRGS) under a grant number FRGS/1/2024/STG06/UNIMAP/02/3.

References

Al Zubi M. 2018. MHD heat and mass transfer of an oscillatory flow over a vertical permeable plate in a porous medium with chemical reaction. *Modern Mechanical Engineering* **8**(03): 179–191.

Aman F., Ishak, A. & Pop I. 2013. Magnetohydrodynamic stagnation-point flow towards a stretching/shrinking sheet with slip effects. *International Communications in Heat and Mass Transfer* **47**: 68–72.

Bejan A. 2013. *Convection Heat Transfer*. 4th Ed. Hoboken, NJ: John Wiley & Sons.

Bhattacharyya K., Mukhopadhyay S. & Layek G.C. 2011. Slip effects on boundary layer stagnation-point flow and heat transfer towards a shrinking sheet. *International Journal of Heat and Mass Transfer* **54**(1–3): 308–313.

Elbashbeshy E.M.A., Asker H.G. & Nagy B. 2022. The effects of heat generation absorption on boundary layer flow of a nanofluid containing gyrotactic microorganisms over an inclined stretching cylinder. *Ain Shams Engineering Journal* **13**(5): 101690.

Hakim K.N.A., Rosali H. & Johari M.A.M. 2023. Stagnation-point flow and heat transfer over an exponentially shrinking/stretching sheet in porous medium with heat generation. *Mathematical Modeling and Computing* **10**(4): 1260–1268.

Ishak A., Nazar R. & Pop I. 2009. MHD convective flow adjacent to a vertical surface with prescribed wall heat flux. *International Communications in Heat and Mass Transfer* **36**(6): 554–557.

Jamrus F.N., Ishak A. & Waini I. 2024. Stability scrutinization of time depending flow of a ternary hybrid nanofluid past a shrinking sheet with wall mass suction effect. *Malaysian Journal of Fundamental and Applied Sciences* **20**(3): 528–543.

Khalil S., Abbas T. & Nawaz R. 2024. Study of hybrid nanofluid flow in a porous medium over an exponentially stretching sheet under Joule heating and thermal radiation: Finite difference. *Nano-Structures and Nano-Objects* **40**: 101350.

Khan A.A., Zaimi K., Sufahani S.F. & Ferdows M. 2020. MHD mixed convection flow and heat transfer of a dual stratified micropolar fluid over a vertical stretching/ shrinking sheet with suction, chemical reaction and heat source. *CFD Letters* **12**(11): 106–120.

Merkin J.H. 1986. On dual solutions occurring in mixed convection in a porous medium. *Journal of Engineering Mathematics* **20**(2): 171–179.

Merkin J.H., Najib N., Bachok N., Ishak A. & Pop I. 2017. Stagnation-point flow and heat transfer over an exponentially stretching/shrinking cylinder. *Journal of the Taiwan Institute of Chemical Engineers* **74**: 65–72.

Nagaraju B., Kishan N., Tawade J.V., Meenapandi P., Abdullaeva B., Waqas M., Gupta M., Batool N. & Ahmad F. 2024. Analysis of boundary layer flow of a Jeffrey fluid over a stretching or shrinking sheet immersed in a porous medium. *Partial Differential Equations in Applied Mathematics* **12**: 100951.

Nield D.A. & Bejan A. 2017. *Convection in Porous Media*. 5th Ed. New York, NY: Springer.

Pop I. & Ingham D.B. (Eds.). 2001. *Convective Heat Transfer: Mathematical and Computational Modelling of Viscous Fluids and Porous Media*. Oxford, UK: Pergamon.

Puspanathan S., Naganthran K., Hashmi M.M., Hashim I. & Momani S. 2024. Numerical investigation of Reiner–Rivlin fluid flow and heat transfer over a shrinking rotating disk. *Chinese Journal of Physics* **88**: 198–211.

Roşca N.C. & Pop I. 2013. Mixed convection stagnation point flow past a vertical flat plate with a second order slip: Heat flux case. *International Journal of Heat and Mass Transfer* **65**: 102–109.

Shahzad T., Munir S., Salahuddin T. & Awais M. 2024. Numerical insights of heat and mass transfer in a Darcy-Forchheimer porous space subjected to MHD dissipative stagnation point flow of cross nanofluid towards a melting stretching cylindrical surface. *International Communications in Heat and Mass Transfer* **159**: 108088.

Vafai K. (Ed.). 2015. *Handbook of Porous Media.* 3rd Ed. Boca Raton, FL: CRC Press.

Vajravelu K. & Nayfeh J. 1992. Hydromagnetic convection at a cone and a wedge. *International Communications in Heat and Mass Transfer* **19**(5): 701–710.

Wang C.Y. 2008. Stagnation flow towards a shrinking sheet. *International Journal of Non-Linear Mechanics* **43**(5): 377–382.

Weidman P.D., Kubitschek D.G. & Davis A.M.J. 2006. The effect of transpiration on self-similar boundary layer flow over moving. *International Journal of Engineering Science* **44**(11-12): 730–737.

Centre of Excellence for Social Innovation and Sustainability (CoESIS)
Department of Mathematical Sciences
Faculty of Intelligence Computing
Universiti Malaysia Perlis
02600 Arau,
Perlis, MALAYSIA
E-mail: khairy@unimap.edu.my, fatinnabila@unimap.edu.my*

KCAET Khairpur Mir's
Sindh Agriculture University,
Tandojam, Sindh, PAKISTAN.
E-mail: balochliaqatali@gmail.com

Department of Mathematics and Social Sciences
Sukkur IBA University
Sukkur, PAKISTAN
E-mail: ubaidullah@iba-suk.edu.pk

Department of Mathematics and Statistics
Faculty of Applied Sciences and Technology
Universiti Tun Hussein Onn Malaysia,
Johor, MALAYSIA
E-mail: suliadi@uthm.edu.my

Research Group of Fluid Flow Modelling and Simulation
Department of Applied Mathematics
University of Dhaka
Dhaka, BANGLADESH
E-mail: ferdows@du.ac.bd

Received: 4 March 2025
Accepted: 7 October 2025

*Corresponding author